AN AUTOMATED PARALLEL IMAGE REGISTRATION TECHNIQUE BASED ON THE CORRELATION OF WAVELET FEATURES*

Jacqueline Le Moigne

Applied Information Sciences Branch

NASA/Goddard Space Flight Center - Code 935

Greenbelt, MD 20771

Tel: (301) 286-8723 - Fax: (301) 286-1776

lemoigne@backserv.gsfc.nasa.gov

William J. Campbell

Applied Information Sciences Branch

NASA/Goddard Space Flight Center - Code 935

Greenbelt, MD 20771

Tel: (301) 286-8785 - Fax: (301) 286-1776

campbell@backserv.gsfc.nasa.gov

and

Robert F. Cromp

ABSTRACT

With the increasing importance of multiple platform/multiple remote sensing missions, fast and automatic integration of digital data from disparate sources has become critical to the success of these endeavors. Our work utilizes maxima of wavelet coefficients to form the basic features of a correlation-based automatic registration algorithm. Our wavelet-based registration algorithm is tested successfully with data from the NOAA Advanced Very High Resolution Radiometer (AVHRR) and the Landsat/Thematic Mapper (TM), which differ by translation and/or rotation. By the choice of high-frequency wavelet features, this method is similar to an edge-based correlation method, but by exploiting the multi-resolution nature of a wavelet decomposition, our method achieves higher computational speeds for comparable accuracies. This algorithm has been implemented on a Single Instruction Multiple Data (SIMD) massively parallel computer, the MasPar MP-2, as well as on the CrayT3D, the Cray T3E and a Beowulf cluster of Pentium workstations.

1. REGISTRATION OF SATELLITE REMOTE SENSING IMAGERY

1.1 Why Geo-Registration

Digital image registration is very important in many applications of image processing, such as medical imagery, robotics, visual inspection, and remotely sensed data processing [1,2]. For all of these applications, image registration is defined as the process which determines the most accurate match between two or more images acquired at the same or at different times by different or identical sensors. Registration provides the "relative" orientation of two images (or one image and other sources, e.g., a map), with respect to each other, from which the absolute orientation into an absolute reference system can be derived. Image registration is usually motivated by such goals as object recognition, model matching, pose estimation, or change detection. In this paper, we will only refer to remote sensing applications, for which automated image geo-registration has become a highly desirable technique.

In the near future, satellite remote sensing systems will provide large amounts of global coverage and repetitive measurements representing multiple-time or simultaneous observations of the same features by different sensors. Also, with the new trend of smaller missions, most sensors will be carried on separate platforms, resulting in a tremendous amount of data that must be combined. In meeting some of the NASA/Earth Science Enterprise objectives [2], the combination of all these data at various resolutions - spatial, radiometric and temporal - will allow a better understanding of Earth and space science phenomena. For example, for land cover applications, the combination of coarse-resolution viewing systems for large area surveys and finer resolution sensors for more detailed studies offer the multilevel information necessary to accurately assess the areal extent of important land transformations. High-resolution sensors, such as Landsat or SPOT are very good for monitoring vegetation changes, e.g., changes in forest cover [3-7], when landscape features are local in scale. However, studies at a global or continental scale at high spatial and temporal resolutions would require the processing of very large volumes of data. It is therefore necessary to combine information from both types of sensors to conduct feasible, accurate studies.

Summarizing the different applications of geo-registration, the different categories defined by [1] can be described in terms of remote sensing applications and include:

(1) data fusion, new sensor calibration [8], or *multimodal registration* which enables the integration of complementary information from different sensors as well as super-resolution [9];

(2) change detection [10,11], and Earth resources surveying, or *temporal registration* performed to monitor and measure agricultural, geological or land cover features extracted from data obtained

from one or several sensors over a period of time. Cloud removal is another application of temporal registration, when observations over several days can be fused to create cloud-free data;

(3) landmark navigation, formation flying and planet exploration, or *viewpoint registration* which integrates information from one moving platform or multiple platforms flying together into three-dimensional models; and

(4) content-based [12] or object searching, map updating, or *template registration* which looks for the correspondence between new sensed data and a previously developed model or dataset.

All these examples illustrate how geo-registration is a critical process, and how the amount of data which will have to be registered in the future will grow exponentially. Some of the examples also show that registration will need to be performed in real-time and often without human intervention. These two last remarks bring us to the issue of automatic geo-registration: the final goal of our work is to design fast and accurate methods for the automatic registration of multi-sensor remotely sensed data. The scope of this paper represents the first step towards this future goal, showing how wavelets can be integrated in the registration process, demonstrating it with examples from a few Earth remote sensing sensors, and implementing this algorithm on high-performance parallel computers.

1.2 Why Automatic Geo-Registration

Automatic image registration, which has been extensively studied in other areas of image processing, is still a complex problem in the framework of remote sensing. Often, the most common approach to registration is to extract a few outstanding characteristics of the data, which are called *control points* (CP's), *tie-points*, or *reference points*; then the CP's in both images are matched by pair and used to compute the coefficients of a bivariate polynomial, usually of degree three maximum. In some cases, the CP's are recorded geographic features, also known as Ground Control Points (GCP's), but sometimes the CP's correspond to high-contrast data points (such as crossroads, bends in rivers). Most available systems follow this registration approach, often assuming some interactive choice of the CP's, and those systems are not well suited for the automatic processing of a large number of data, because polynomials require either a few very accurate control points or many inaccurate ones, but well-distributed over the image. In both cases, it is obvious that such a point selection represents a repetitive and labor-intensive task and becomes prohibitive for very large amounts of data. Also, this approach is unpractical when the registration has to be done in real-time, for example for navigation purposes.

Another issue of automatic geo-registration is accuracy. Since the interactive choice of control points in satellite images is sometimes difficult, too few points, inaccurate points, or ill-distributed points might be chosen, and as a result, large registration errors created. Such errors lead to data analysis errors as shown in two studies reported in [13,14]. The two studies demonstrate that a small error in registration may have a large impact on the accuracy of global change measurements and that, for example, a registration accuracy of less than 0.2 pixel is required to achieve change detection errors of less than 10%.

As a summary, for reasons of speed, portability, and accuracy, automatic geo-registration is an important requirement to ease the work load, speed up processing, and improve the accuracy in locating a sufficient number of well-distributed accurate tie-points. Such a technique can also be integrated in an hybrid automatic-manual cooperative registration which is preferred for some applications.

In the remainder of this paper we briefly review previous automatic registration methods, then we describe how to utilize wavelets for registration purposes and the parallel implementation of such a wavelet-based algorithm. Finally, some results are presented and future work is described.

2. REGISTRATION - A BRIEF SURVEY

2.1 Which Distortions Must be Corrected

The distortions described in [15] for Landsat-MSS data are general enough to account for most sensors directed at the Earth. Distortions are defined by the combined effects of sensor operation, the Earth's rotation, orbit and attitude anomalies and atmospheric and terrain effects. These distortions, which are noticeable when dealing with only one sensor, are even larger when considering multiple sensors carried by multiple platforms on different orbits. Refer to [15,16] for a good description of distortion sources and distortion categories. Distortions of airborne sensors are also described in [17].

In this paper, we will assume that distortions relative to sensor operation, Earth's rotation, and atmospheric effects have been corrected as part of a "systematic" correction. As a first approximation, we will only be dealing with "precision" correction for orbit and attitude anomalies. This type of distortion mainly corresponds to an affine transformation. A few other

small continuous non-linear distortions due to altitude, velocity, yaw, pitch, and roll could be handled by global or local polynomial transformations of higher degree.

2.2 Registration Steps and Issues

We assume that any new incoming *sensed* image is being registered relative to a known *reference* image. We also assume that *sensed image* and *input image* are synonymous. According to Brown [1], image registration can be viewed as the combination of four components:

(1) *a feature space, i.e.* the set of characteristics used to perform the matching and which are extracted from reference and input data;

(2) *a search space, i.e.* the class of potential transformations that establish the correspondence between input data and reference data;

(3) *a search strategy,* which is used to choose which transformations have to be computed and evaluated; and

(4) *a similarity metric,* which evaluates the match between input data and transformed reference data for a given transformation chosen in the search space.

The transformation which gives the best match according to the similarity measure is also called the *deformation model* or the *mapping function.* According to some a priori knowledge of the data, different search spaces may be chosen. For the reasons given in section 2.1, transformations that are often used are *rigid transformations* (composed of a scaling, a translation and a rotation), *affine transformations* (composed of a rigid transformation, a shear and an aspect-ratio change; a shear in the x-axis transforms the x-coordinate into a linear combination of both x and y-coordinates, and the aspect-ratio is defined as the numerical ratio of image width to height), and polynomial transformations. Correlation measurement is the usual similarity metric [18], although it is computationally expensive and noise sensitive when used on original gray level data; using a multi-resolution search strategy enables large reductions in computing time and increases the robustness of the algorithms. Other similarity metrics are described in [19], and a comparison of isometric (which preserves distances) versus polynomial transformations is given in [20]. Although high-order polynomials are superior to isometric transformations when the deformation includes more than a translation and a rotation, isometric transformations are more accurate when a smaller number of points is available and are less sensitive to noise and to largely inconsistent tie-points. Several feature extraction and feature matching methods have been integrated and compared in a system developed by Rignot et al [21]. Most previous methods are applied on an image-to-image basis, i.e. band-to-band of multivariate data.

Another way to classify registration methods is adopted by Fonseca et al. [11], where twelve recent registration methods are described according to the type of their feature extraction. Automatic feature extraction is either area-based or feature-based, the feature-based process occurring either in the spatial domain or in the transform domain.

In this section, we will take another viewpoint to describe a majority of the registration methods found in the literature in the past thirty years, and which have the potential to be applied to remote sensing images. As previously described, a usual semi-manual registration first manually determines corresponding control points before computing the deformation model. Automatic methods can be classified into two types, those which follow a human approach, with a point-to-point matching, and those which take a global matching approach. In section 3, we describe a two-step approach in which the first step does not rely on point to point matching of control points to compute a first estimate of the mapping function.

Among the methods which perform point-to-point matching [22-41], the most common control points are the centers of gravity of regions (Cracknell [24], Flusser [27], Goshtasby [29,30], Li et al [38], Ton [23], Ventura [34]) with or without region attributes such as areas, perimeters, ellipticity criteria, affine-invariant moments [40], and inter-regions distances. More recently, several authors (Corvi [25], Djamdji [26,41], Li&Zhou [32,39], Chellappa et al [35,36]) have been using features extracted from a wavelet decomposition. Some examples are maxima and minima of wavelet coefficients, high-interest points or local curvature discontinuities. A few methods [17] utilize Delaunay triangulation methods to progressively increase the number of accurate control points. The main difficulty associated with point-to-point matching occurs with missing or spurious points, which makes the matching process more difficult and less reliable [9,20,22,23].

Among the global methods [9,19,42-54], the transformation is either found by correlation or by optimization, in the spatial or in the frequency domain. When in the spatial domain, correlation or optimization is performed either in the original data or on edge gradient data. Another method proposed by Stockman [49] involves the computation of a "Hough accumulator" for all the transformations matching edge segments or vectors linking feature points. Some recent research (Thevenaz and Unser [42,50]) has also focused on the use of wavelets for global image registration.

Other more recent methods are also described in [55]. We qualitatively compare our work to all the registration methods based on wavelet transforms in section 3. Section 4 describes how the first step of this approach has been implemented on parallel computers, while section 5 shows results of our technique applied to several remote sensing image data.

3. REGISTRATION USING WAVELETS

Our goal is to define fast, accurate methods for the automatic registration of remotely sensed data. The accuracy of these methods will be defined by the choice of the search strategy (component 3 in the registration definition), which could itself be a component of a general planning strategy [56] choosing a trade-off between accuracy and speed of the proposed methods according to the user's needs.

To solve the problem of missing or spurious points in the matching process, we propose to solve the registration problem in two steps:

Step 1   The mapping function is computed globally over the images, without individual matching of control points. This step provides a good first estimate of the mapping function, chosen in this work as a composition of rotations and translations.

Step 2   Many strong and well-distributed features are extracted throughout the images and the previous transformation is utilized to perform the matching. Sub-pixel accuracy can be achieved if the number of matched pairs is much larger than the minimum number required to compute the final deformation model.

In this paper, we will focus on step 1 with an emphasis on the computational speed and on the ability of the developed techniques to handle multi-sensor data; these two requirements brought us to the utilization of multi-resolution wavelet transforms. Briefly, a wavelet decomposition of any given signal (1-D or 2-D) is the process which provides a complete representation of the signal according to a well-chosen division of the time-frequency (1-D) or space-frequency (2-D) plane. Through iterative filtering by low-and high-pass filters, it provides information about low- and high-frequencies of the signal at successive spatial scales. See references [57-61] for more detail on wavelet transforms. The choice of using wavelets is justified by the following reasons:

(1) Multi-resolution wavelets, largely used for data compression and browsing, are used as a first step to bring the multiple types of data to the same resolution without losing significant information and without blurring the higher resolution data. Multi-resolution wavelet decomposition preserves most of all important features of the original data even at a lower resolution, especially global scale features such as rivers, roads, and lakes.

(2) Further multi-resolution wavelet decomposition highlights strong image features at the lower resolution thus eliminating weak higher resolution features.

(3) The multi-resolution iterative search focuses progressively towards the final transformation with a search interval decreasing and an accuracy increasing at each iteration. This algorithm achieves higher accuracies with higher speeds than a full search at full resolution.

(4) Multi-resolution wavelet transforms can be implemented very easily on a parallel computer.

3.1 Choice of Wavelet Coefficients

Different choices of wavelet transforms can be made; we chose to use orthonormal wavelets. The main advantage of orthonormal wavelets is their computational speed, but their main disadvantage is their lack of translation-invariance, which means that the wavelet transform does not commute with the translation operator. According to the Nyquist criterion, in order to distinguish between all frequency components and to avoid aliasing, the signal must be sampled at least twice the frequency of the highest frequency component; therefore when using a separable orthogonal wavelet transform, information about the signal may change within or across subbands [64]. In order to assess the useability of orthonormal wavelets for image registration, we conducted a study where the use of wavelet subbands was quantitatively assessed as a function of features' sizes. This study reported in Stone et al [62] shows that using cross-correlation and orthogonal wavelet filters is still a useful registration scheme in spite of translation effects. The results are summarized here, see [62] for more details:

• the low-pass subband is relatively insensitive to translation, provided that the features of interest have an extent at least twice the size of the wavelet filters.

• the high-pass subband is more sensitive to translation, but the peak correlations are still high enough to provide an accurate registration.

From the experiments reported in this paper, we also observed that a local lack of translation invariance is compensated by taking a global approach instead of a point-to-point matching, and by the combination of information from several image subbands. To further investigate this issue, other translation-invariant wavelet transforms [63-65,75] are now being studied.

According to Mallat [61], an orthonormal basis of wavelets can be defined by a scaling function and its corresponding conjugate filter L. In this case, the wavelet decomposition of an image is similar to a quadrature mirror filters decomposition with the low-pass filter L and its mirror high-pass filter H; this decomposition is summarized in Figure 1. The filters L and H are one-dimensional of varying size depending on the application (see [59] for more detail). For registration purposes, we have tested all filter sizes between 2 and 20 and have found 4, 6, or 8 to be the most useful filter sizes. Below size 4, the size 2-Haar filter might create step edges in the filtered data,

while above size 8, edge blurring occurs. We will call LL, LH, HL and HH the four sub-images (or subbands) created at each level of decomposition.

In order to choose which wavelet coefficients to use for registration purposes, we first applied this wavelet decomposition to the image of a human face, where strong features are easy to extract visually. Results, reported in (Le Moigne [66,67], show that the strongest features appear in either one of the two bands LH or HL, with the Low/High (LH) band emphasizing horizontal features of the signal and the High/Low (HL) band emphasizing vertical characteristics. The High/High (HH) subband theoretically corresponds to diagonal features, but as can be seen in [66], the information contained in the HH subband also includes a large proportion of high-frequency noise. Further work on the use of the different subbands can also be found in our related work [62]. From these observations, we chose to utilize the maxima of the LH and HL bands as the feature set of our registration algorithm.

3.2 Idea of the Algorithm

According to the registration framework given by Brown[1], our algorithm can be described by the four following components:

1. The feature space

After performing the wavelet decomposition of both reference and input images, the histograms of LH and HL images are computed for all levels of decomposition. Then, only those points whose intensities belong to the top $x\%$ of the histograms are kept (x being a parameter of the program whose selection can be automatic); we call these points "maxima of the wavelet coefficients" (or "maxima"), and these maxima form the feature space. We will see in section 5.1 that when x is automatically selected, its value varies between 13% and 15%.

2. The search space

The search space is composed of 2-D rotations and translations. Unless otherwise specified by the user, the system looks for rotations with angles included in the interval [0,90degrees] and for translations in the interval [0, half-the-maximum-dimension-in-the-reference-image]; more generally, the search can be reduced by utilizing a-priori information about the sensor movement and the satellite navigation system, as well as their corresponding accuracies.

3. The search strategy

The search strategy follows the multiresolution approach provided by the wavelet decomposition. At the highest level of decomposition, the search is exhaustive over the whole

search space but with an accuracy equal to Δ. The first approximation of the best rotation, R_n, is chosen over this search space; then R_n becomes the center of a new search interval of length 2Δ, $[R_n - \Delta, R_n + \Delta]$, and at the next lower level, the new approximated rotation, R_{n-1}, is found within this search interval with an accuracy of $\Delta/2$. This process is repeated until the first level of wavelet decomposition, where the search interval is $[R_2 - \Delta/2^{n-2}, R_2 + \Delta/2^{n-2}]$ and the final registration rotation, R_1, is found with an accuracy equal to $\Delta/2^{n-1}$. In particular, if δ is the desired registration accuracy, Δ is chosen as $2^{n-1}\delta$, where n is the number of levels of wavelet decomposition. Table 1 summarizes this search strategy, and Table 2 summarizes the algorithm for four levels of decomposition, an image of size 512x512, a search for rotations, and an initial accuracy, Δ, equal to 10 degrees.

In some cases, for reasons of robustness, even if the final desired accuracy δ does not require Δ to be small at the lowest resolution level, smaller accuracy steps can be considered for the initial step, and then the previous process described in Table 1 can be applied starting at level n-1, once the initial approximation of the transformation has been computed. This strategy avoids pursuing a false path in the search for the optimal transformation. Other authors [51] have proposed to simultaneously pursue several paths, but this requires more computations.

Similarly, in the case of a composition of a rotation and a translation, the search is performed simultaneously on the three parameters, rotation angle, shift in x-direction and shift in y-direction. To reduce the amount of computations, another solution is shown in Table 3 where the search over three parameters is decomposed at intermediate levels into two searches in the complementary sub-spaces, sub-space of translations and sub-space of rotations. At each intermediate level of decomposition, the rotation is first assumed to be known and the translation is refined, then the translation is assumed to be known and the rotation is refined. Decomposing the main search into two "sub-searches" reduces dramatically the amount of computations, as shown in Table 3. A first approximation of the scale can be found by utilizing a Fourier-Mellin transform [46] or a log-polar transform [77] that transform the search for rotation or scale into a search for translation in the new transformed space. Once an approximation of the scale is found, a similar approach using "sub-searches" can be taken when searching for a rigid or an affine transformation.

4. The similarity metric

The similarity metric of our registration algorithm is a cross-correlation measure. At each level, the best transformation is found by computing the successive correlations between wavelet coefficients of the input image and transformed wavelet coefficients of the reference image. The

transformation which corresponds to the highest correlation is chosen as the center of the next search interval.

The registration algorithm is then described as follows:

(A) Wavelet Decomposition of Reference Image.

(B) Wavelet Decomposition of Input Image. Find maxima of LH and HL coefficients for each level of decomposition after histogram computation.

(C) Starting from last level of decomposition and then iteratively for each level going up, find the best match between maxima of wavelet coefficients of input image and rotated and/or translated maxima of the wavelet coefficients of the reference image. The best transformation is then refined iteratively and with increasing accuracy, as previously described.

Compared to an edge-based correlation performed on the original data which would require 360 floating point operations per pixel, our wavelet-based registration only requires 110 floating point operations per pixel.

Unlike our method, most wavelet-based registration approaches (as described in section 2.2) utilize a control-point matching approach, except for the methods described by Thevenaz and Unser [42,50] and by Olivo [48], which differ either by the type of wavelets, the type of features and/or the similarity metric, as well as by the application domain. A feature space similar to ours is used by Corvi [25] and Djamdji [26], although Corvi also uses wavelet minima. Djamdji's approach also differs by the type of wavelet decomposition, which is an "algorithme a trous" with a non-decimating approach. Li and Zhou [32,39] compute multi-resolution edges and high-interest points on these contours to perform the matching. Zheng and Chellappa [36] utilize a multi-resolution Gabor wavelet, the maxima of an energy measure to find local curvature discontinuities and a local correlation on windows around these maxima to perform the point-to-point matching. The latter two methods have been mainly tested on aerial and SAR imagery.

We have tested our method on several scenes of remote sensing imagery (as well as human face images, see [66]). Our approach is summarized by the following characteristics:
- the matching is performed globally instead of point by point which, in the absence of a-priori knowledge, decreases the risk of computing a match based on too few inaccurately paired points;
- the search strategy takes advantage of the multi-resolution decomposition to speed up the process and to reduce the effect of noise, since lowering image resolution removes high-frequency noise;
- the matching is computed on significant features (the maxima) instead of all pixels, which increases the control of the algorithm over noise, and reduces computation time; and

- the tuning of parameters is minimal. The only parameter, x, which controls the number of maxima chosen from the histograms, can be computed adaptively within the program, as will be explained in section 5.1.

4. PARALLEL IMPLEMENTATION

Since both the need for image registration and the amount of data to register are going to grow tremendously in the near future, the implementation of automatic image registration methods on high-performance computers needs to be investigated. For this reason, our algorithm has been implemented on a massively parallel computer, the MasPar MP-2, as well as on other parallel computers [68-70]. The MasPar Parallel Processor is a fine-grained, massively parallel computer with a Single Instruction Multiple Data (SIMD) architecture, consisting of 16,384 parallel processing elements arranged in a 128x128 matrix and connected by an eight nearest neighbors interconnection network. The reasons for using a MasPar were two-fold: first, the MasPar was very easily accessible to our research group, second a SIMD architecture is very appropriate to the computation of wavelet decomposition, which is essentially a pixel-parallel type processing. Other tests implementing a wavelet decomposition using a Cray T3D, an Intel Paragon, a Beowulf computer and a Convex SPP are reported in [68] and show that the MasPar provides the best speed-up, followed by the Cray T3D and then the Beowulf computer. The Beowulf, a Commercial-Off-The-Shelf (COTS) parallel computer, is a cluster of PC's running parallel Linux.

Wavelet decomposition, using a succession of convolution and decimation operations, is implemented in a straightforward fashion on a parallel architecture. Four consecutive pixels are stored into four layers of the same Processing Element (PE), convolutions are performed simultaneously at each PE and decimation is easily obtained by considering only half the number of layers at each iteration. For a 512x512 image, a filter size 4, and four decomposition levels, the computing time on the MasPar MP-2 is approximately 0.0154 seconds, compared to 4.87 seconds for the sequential timing which represents an improvement of about 300. Table 4 shows some other timing performances on the MasPar with different filter sizes. The results on the Beowulf (1.34 seconds) are very comparable to those obtained on the Cray T3D (0.75 seconds), which is very encouraging for such a COTS-type architecture. See El-Ghazawi et al [68] and Chan et al [69] for more details on the parallel implementation of the wavelet decomposition.

As described previously, for registration purposes, maxima of the LH and HL wavelet coefficients are found by computing the histograms of these two images, and choosing for each

image a threshold such that the thresholded images contain at most $x\%$ of the total number of points in the image. For the above test, histogramming and thresholding are computed in 0.38 seconds on the MasPar. The new locations of the rotated pixels are computed in parallel on all the pixels. Each rotation takes about 0.02 seconds for an image up to 128x128 (since the MasPar array is of size 128x128), and 0.04 seconds for a 256x256 image. No complete systematic study of the implementation of the wavelet-based registration was performed on the MasPar, but further studies on the implementation of this registration on other parallel computers are reported in [70]. Table 5 shows some of these results. On the Beowulf architecture, the algorithm requires about 0.545 seconds when 16 processors are utilized, while it takes 0.196 seconds on the Cray T3E and 0.52 seconds on the Cray T3D, for the same number of processors. In general, Beowulf shows similar or better performances than the Cray T3D. Furthermore, although Cray T3D and Cray T3E show better scalability than Beowulf, Beowulf still exhibits a speed-up of 8 for 16 processors, which shows a good ratio performance versus cost compared to other processors. See [70] for more details on these results.

5. RESULTS

Results are shown using Landsat Thematic Mapper (see Figure 2), and AVHRR (see Figures 5 and 6) data. For all the examples below, nearest neighbor was used as the common resampling function.

5.1 Landsat/TM

Figure 2a is a 512X512 image extracted from Band 2 of a Landsat-TM scene of the Pacific Northwest. Figure 2c shows Figure 2a rotated 18 degrees; this rotation has been computed independently to test the results given by our algorithm. Figures 2b and 2d show the four levels of wavelet decomposition of Figures 2a and 2c, respectively, using a Daubechies filter size 4, and four levels of decomposition. Figure 2a (straight) is taken as the reference image, and Figure 2c (rotated) is considered as the sensed image. Figure 3 shows at each level the maxima which form the feature space, and the rotations of these maxima for the reference image. We chose to perform the registration with a final accuracy of 1 degree ($\delta=1$) which, according to Table 1, imposes the initial search space to be [0,88] and the initial accuracy (or increment) to be 8 degrees ($\Delta=8$). Then the successive search spaces and accuracies follow the principle given in Table 2, according to the best rotations found at each step. The final correct rotation is retrieved as 18 degrees.

The best rotation at each level is chosen as the one maximizing the sum of the correlation between LH bands and the correlation between HL bands. The correlation results are illustrated in Figure 4; these graphs show how the two correlation functions LH and HL are quite different at the lowest level although they share the same maximum; it shows that at this level, computing the sum of the two correlation measures is very useful to choose a local maximum. Then, as the search focuses more and more around the final transformation, the two curves become more and more similar, and are almost identical at the highest level of decomposition. These results suggest that as soon as the search space has been narrowed around the final transformation, only one of the two functions LH or HL could be utilized, thus reducing by half the amount of computation.

Another issue to consider is the determination of the parameter x which defines the number of maxima in each image. As shown in Table 6, this parameter can be computed adaptively by the program; at the lowest level of resolution, the best transformation is computed successively for the four values 5%, 10%, 15%, and 20% of x. A correlation measure is associated to each of these four computations. Then the parameter x is chosen as the sum of these four thresholds weighted by their corresponding correlations:

$$x\% = 5\% * Correl_{5\%} + 10\% * Correl_{10\%} + 15\% * Correl_{15\%} + 20\% * Correl_{20\%} .$$

This formula has been chosen after a few experiments that showed that below 5% too few features remain in the images, and above 20% too much noise is taken into account. Table 6 shows example details for the computation of the parameter x with different rotations and translations. For these examples, the adaptive value of x varies between 13% and 15%. Since noise is higher in higher resolution data, we have experimentally found it most effective to decrease x by an additional 2% for each higher level of decomposition.

Other experiments were performed using Figure 2 as well as a test portrait image shown in reference [66]. Both images were artificially transformed by a series of rotations and translations: results are shown in Table 7. Compared to other simple correlation-based methods such as spatial correlation, phase correlation, and edge-based registration, the results show that wavelet-based registration performs as well or better than the other methods, and that the average rotation error over these examples is 0.42 degrees and the average translation error is 0.17 pixels.

5.2 AVHRR/LAC

Figure 5 and Table 8 present results obtained with a 512x512 AVHRR-LAC image of the Pacific Northwest area, which has been independently rotated by 5 degrees and translated by 10 columns and 6 rows. Figure 5 shows the original image. The wavelet decomposition was performed

using a Daubechies size 4 filter. At the lowest level of decomposition, the previous adaptive search is performed, leading to a threshold of 11% for level 3; then at each level, this threshold is automatically decreased by 2%. At the lowest level, for a better robustness, as described in section 3.3, the search is performed with increments of 4 degrees in rotations and 4 pixels in translations. Then, from level 3 up, the search strategy described in Table 1 is applied with final accuracies of 1 degree in rotations and 1 pixel in translations. After the search is completed, a rotation of 5 degrees and a translation of (5.00,3.00) pixels are found in the 256x256 image; this result is interpolated as a rotation of 5 degrees and a translation of (10.00,6.00) pixels in the full 512x512 image.

Other results were obtained with an AVHRR dataset which represents a series of thirteen 512 rows by 1024 columns AVHRR/LAC images over South Africa, navigated and georeferenced to a geographic grid using an orbital model developed at the University of Colorado [71] which assumes a mean attitude behavior (roll, pitch and yaw) derived using Ground Control Points [72]. A map of the coastline derived from the Digital Chart of the World (DCW) was generated for the same geographic grid, and was used to visualize the registration before and after our process. Figure 6 shows this dataset. Since no registration ground truth was available for these images, all data have been manually registered, assuming only a translation transformation. The results of the manual registration have been verified by superimposing the binary map of the coastlines onto the respectively shifted images (see Figure 7). Most of the results obtained by manual registration are verified as accurate by the coastline map. But for some of the data, especially very cloudy images, manual results do not match the coastline map and cannot really be considered as "ground truth" but only as "references" for accuracy purposes. Figure 7 shows some of the results of our registration algorithm superimposed with the coastline. Overall the differences of registration between the manual registration and our wavelet-based algorithm average 1.43 pixels and 1.05 pixels if the two most cloudy scenes, sa143 and sa146, are not included in this computation (see Table 9).

Since misregistration errors occur mainly for cloudy scenes, we can use the knowledge of the coastline to create a mask and reduce the search for the correct transformation in an area along the coastline. In this last test, the consistency of the algorithm [78] is checked by looking in an area of [-40,+40] pixels in the vicinity of the coastline and by performing inter-registration of all pairs of scenes. From all these permutations of registrations, an average translation error is computed by considering the sum of the errors on all triplets of scenes. After these computations, the average translation error is of 0.425 pixels, which demonstrates sub-pixel consistency of our method.

More generally, on-going experiments are being performed to assess the accuracy of our algorithm as a function of translation and rotation amounts as well as a function of noise [79].

6. CONCLUSION

We have presented a method for image registration based on wavelet decomposition and correlation, which shows promising results for fast registration of digital remotely sensed images. The characteristic features of the images are computed automatically through wavelets and the matching is done globally over the image, instead of locally for each pair of control points. The deformation model is assumed to be the composition of a rotation and a translation. For rigid and affine transformations, the approach can be generalized by using sub-searches or by replacing the exhaustive search by an optimization or a statistically robust feature matching [73,74]. One of the main advantages of this approach is its ease of implementation on high-performance parallel architectures, such as the massively parallel computer, MasPar MP-2, or a Beowulf cluster of workstations.

The final step of the algorithm will utilize this first global transformation to locate and match automatically a few accurate reference points in the high resolution data and will refine locally the transformation. In a multi-resolution/multi-sensor framework, wavelet decomposition is first utilized to bring both sets of data to the same resolution, then it is used for registration purposes [76].

Future work will also include the study of other types of wavelets, the integration of cloud masks, when available, and a quantitative evaluation of our method relative to different test data as well as compared to other registration techniques; a first evaluation was performed [73] and will be continued. Automatic registration of remotely sensed data is a very complex problem, and as stated by other authors [11,21], we feel that only a future system that integrates multiple automated registration techniques will be able to address such a task for multiple types of remote sensing data.

ACKNOWLEDGEMENTS

REFERENCES

1. L. Brown, "A Survey of Image Registration Techniques," *ACM Computing Surveys*, Vol. 24, No. 4, 1992.

2. *Exploring Our Home Planet, Earth Science Enterprise, Strategic Plan*, National Aeronautics and Space Administration, January 2001.

3. J.P. Malingreau, C.J. Tucker, and N. Laporte, "AVHRR for Monitoring Global Tropical Deforestation," *International Journal of Remote Sensing*, Vol. 10, Nos. 4&5, pp. 855-867, 1989.

4. V.V. Salomonson, W.L. Barnes, P.W. Maymon,H.E. Montgomery, and H. Ostrow, "MODIS: Advanced Facility Instrument for Studies of the Earth as a System," *IEEE Transactions Geoscience and Remote Sensing*, Vol. 27, 145-153, 1989.

5. D. Skole, and C.J. Tucker, "Tropical Deforestation and Habitat Fragmentation in the Brazilian Amazon: Satellite Data from 1978 to 1988," *Science*, Vol. 260, 1905-1910, 1993.

6. J.R. Townshend, C.O. Justice, "Selecting Spatial Resolution of Satellite Sensors Required for Global Monitoring of Land Transformations," *International Journal of Remote Sensing*, Vol. 9, No.2, 187-236, 1988.

7. *Improved Global Data for Land Applications, A Proposal for a New High Resolution Data Set. Report of the Land Cover Working Group of IGBP-DIS*, Global Change Report No. 20, ed. J.R.G. Townshend, 1992.

8. G.J. Jedlovec, and R.J. Atkinson, "Calibration, Navigation, and Registration of MAMS Data for FIFE," *NASA-TM-108397*, 1993.

9. M. Irani, and S. Peleg, "Improving Resolution by Image Registration," *Computer Vision, Graphics, and Image Processing*, Vol. 53, No.3, 213-239, 1991.

10. D. Yuan, C.D. Elvidge, J.G. Lyon, and R.S. Lunetta, "North America Land Cover Change Detection Using Historical MSS Data: Three Pilot Studies," *Proceedings ECO RIO'94, International Symposium on Resource and Environmental Monitoring*, Rio de Janeiro, Brazil, 1994.

11. L.M.G. Fonseca, and B.S. Manjunath, "Registration Techniques for Multisensor Sensed Imagery," *Photogrammetric Engineering and Remote Sensing Journal*, Vol. 62, No. 9, 1049-1056, Sept. 1996.

12. R.F. Cromp, and W.J.Campbell, "Data Mining of Multidimensional Remotely Sensed Images," in *Proceedings of 2nd International Conference in Information and Knowledge Management*, Washington, D.C, 471-480, 1993.

13. J. Townshend, C.O. Justice, C. Gurney, and J. McManus, "The Impact of Misregistration on Change Detection," *IEEE Transactions on Geoscience and Remote Sensing*, Vol. 30, No. 5, 1992.

14. X. Dai and S. Khorram, "The Effects of Image Misregistration on the Accuracy of Remotely Sensed Change Detection," *IEEE Transactions on Geoscience and Remote Sensing*, Vol. 36, No.5, September 1998.

15. P. Van Wie, and M. Stein, "A Landsat Digital Image Rectification System," *IEEE Transactions on Geoscience Electronics*, Vol. GE-15, No. 3, 130-137, 1977.

16. J.A. Richards, *Remote Sensing Digital Image Analysis: An Introduction,* Springer-Verlag, 2nd Edition, 1993.

17. B.J. Devereux, R.M. Fuller, L. Carter, and R.J. Parsell, "Geometric Correction of Airborne Scanner Imagery by Matching Delaunay Triangles," *Int. J. Remote Sensing*, Vol. 11, No. 12, 2237-2251, 1990.

18. W.K. Pratt, "Correlation Techniques of Image Registration," *IEEE Transactions on Aerospace and Electronic Systems,* Vol. AES10, No. 3, 353-358, 1974.

19. D.I. Barnea, and H.F. Silverman, "A Class of Algorithms for Fast Digital Registration," *IEEE Transactions on Computers*, Vol. C-21, 179-186, 1972.

20. Y.C. Hsieh, D. McKeown, and F.P. Perlant, "Performance Evaluation of Scene Registration and Stereo Matching for Cartographic Feature Extraction," *IEEE Transactions on Pattern Analysis and Machine Intelligence*, Vol. 14, No. 2, 1992.

21. E.J.M. Rignot, R. Howk, J.C. Curlander, and S.S. Pang, "Automated Multisensor Registration: Requirements and Techniques," *Photogrammetric Engineering & Remote Sensing*, Vol. 57, No. 8, 1029-1038, 1991.

22. P.D. Fiore, "Image Registration Using Both Distance and Angle Information," in *International Conference on Image Processing*, Washington, D.C., Oct.23-26, 1995.

23. J. Ton, A.K. Jain, "Registering Landsat Images by Point Matching," *IEEE Transactions in Geoscience and Remote Sensing,* Vol. 27, No. 5, 1989.

24. A.P. Cracknell, and K. Paithoonwattanakij, "Pixel and Sub-Pixel Accuracy in Geometrical Correction of AVHRR Imagery," *International Journal of Remote Sensing*, Vol. 10, Nos. 4,5, 661-667, 1989.

25. M. Corvi, M., and G. Nicchiotti, "Multiresolution Image Registration," in *Proceedings 1995 IEEE International Conference on Image Processing*, Washington, D.C., Oct. 23-26, 1995.

26. J.P. Djamdji, A.Bijaoui, and R.Maniere, "Geometrical Registration of Images. The Multiresolution Approach," *Photogrammetric Engineering & Remote Sensing Journal,* Vol. 59, No. 5, May 1993.

27. J. Flusser, "An Adaptive Method for Image Registration," *Pattern Recognition,* Vol. 25, No.1, 45-54, 1992.

28. J. Flusser, and T. Suk, "A Moment-Based Approach to Registration of Images with Affine Geometric Distortion," *IEEE Transactions on Geoscience and Remote Sensing*, Vol. 32, No. 2, 382-387, 1994.

29. A. Goshtasby, "Registration of Images with Geometric Distortions," *IEEE Transactions in Geoscience and Remote Sensing*, Vol. 26, No. 1, 60-64, 1988.

30. A. Goshtasby, G. Stockman, and C. Page, "A Region-Based Approach to Digital Image Registration with Subpixel Accuracy," *IEEE Transactions on Geoscience and Remote Sensing*, Vol. GE-24, No. 3, May 1986.

31. B. Kamgar-Parsi, J.L. Jones, and A. Rosenfled, "Registration of Multiple Overlapping Range Images: Scenes Without Distinctive Features," *IEEE Transactions on Pattern Analysis and Machine Intelligence*, Vol. 13, No. 9, 857-871, 1991.

32. H. Li, and Y-T. Zhou, "Automatic EO/IR Sensor Image Registration," in *Proceedings 1995 IEEE International Conference on Image Processing*, Washington, D.C., Oct. 23-26, 1995.

33. B. S. Manjunath , C. Shekhar, and R. Chellappa, "A new approach to image feature detection with applications," *Pattern Recognition*, Vol. 29, No. 4, 627-640, 1996.

34. A.D. Ventura, A. Rampini, and R. Schettini, "Image Registration by the Recognition of Corresponding Structures," *IEEE Transactions Geoscience and Remote Sensing*, Vol. 28, No. 3, 305-387, 1990.

35. Y.-S. Zhang, P. Burlina, and R. Chellappa, "Semi- and Fully-Automatic Techniques for Image to Site Model Registration," *IEEE Transactions on Image Processing*, 1996.

36. Q. Zheng, and R. Chellappa, "A Computational Vision Approach to Image Registration," *IEEE Transactions on Image Processing*, vol. 2, p. 311-326, 1993.

37. A.J. Lee, N.H. Carender, D.J. Knowlton, D.M. Bell, and J.K. Bryan, "Fast Autonomous Registration of Landsat, SPOT, and Digital Imagery," *SPIE Aerosense, Integrating Photogrammetric Techniques with Scene Analysis and Machine Vision*, April 11-16, Orlando, 1993, 68-79.

38. H. Li, B.S. Manjunath, and S.K. Mitra, "A Contour-Based Approach to Multisensor Image Registration," *IEEE Transactions on Image Processing*, vol. 4, no. 3, pp. 320-334, 1995.

39. H.H. Li, and Y.-T. Zhou, "A Wavelet-Based Point Feature Extractor for Multi-Sensor Image Registration," in *SPIE Aerosense Wavelet Applications III*, Orlando, Florida, pp. 524-534, 1996.

40. Z. Yang, and F.S. Cohen, "Image Registration and Object Recognition Using Affine Invariants and Convex Hulls," *IEEE Transactions on Image Processing*, Vol.8, No.7, July 1999, 934-946.

41. J.P. Djamdji and A. Bijaoui, "Disparity Analysis: A Wavelet Transform Approach," *IEEE Transactions on Geoscience and Remote Sensing*, Vol. 33, No. 1, January 1995, 67-76.

42. P. Thévenaz, U.E. Ruttimann, and M. Unser, "A Pyramid Approach to Sub-Pixel Registration Based on Intensity," *IEEE Transactions on Image Processing*, Vol.7, pp. 27-41, Jan. 1998.

43. L.-H. Lee, and L.-C. Chen, "A New Method for Automated Control Point Selection in Image Registration," in *Close-Range Photogrammetry Meets Machine Vision*, Zurich, Switzerland, 1990.

44. R.L. Allen, F.A. Kamangar, and E.M. Stokely, "Laplacian and Orthogonal Wavelet Pyramid Decompositions in Coarse-to-Fine Registration," *IEEE Transactions on Signal Processing*, vol. 41, no. 12, December 1993.

45. P. Anuta, P., "Spatial Registration of Multispectral and Multitemporal Digital Imagery Using Fast Fourier Transform Techniques," *IEEE Transactions on Geoscience Electronics*, vol. GE-8, no. 4, October 1970.

46. Q.S. Chen, M. Defrise, and F. Deconinck, "Symmetric Phase-Only Matched Filtering of Fourier-Mellin Transforms for Image Registration," *IEEE Transactions on Pattern Analysis and Machine Intelligence*, vol. 16, no. 12, pp. 1156-1168, 1994.

47. B.D. Lucas, and T. Kanade, "An Iterative Image Registration Technique with an Application to Stereo Vision," in *1981 DARPA Image Understanding Workshop*, April 1981.

48. J.-C. Olivo, J. Deubler, C. Boulin, "Automatic Registration of Images by a Wavelet-Based Multiresolution Approach," in *SPIE Wavelet Applications in Signal and Image Processing III*, San Diego, CA, July 12-14, 1995.

49. G. Stockman, S. Kopstein, and S. Bennett, "Matching Images to Models for Registration and Object Detection via Clustering," *IEEE Transactions on Pattern Analysis and Machine Intelligence*, vol. PAMI-4, no.3, pp. 229-241, 1982.

50. M. Unser, and A. Aldroubi, "A Multiresolution Image Registration Procedure Using Spline Pyramids," in *Proceedings SPIE, Mathematical Imaging: Wavelet Applications in Signal and Image Processing*, San Diego, 1993.

51. Y.F. Wu, and H. Maître, "A Multiresolution Approach for Registration of a SPOT Image and a SAR Image," in *Proceedings of 10th Annual International Geoscience and Remote Sensing Symposium*, pp. 635-638, May 1990.

52. H. Shekarforoush, M. Berthod, and J. Zerubia, "Subpixel Image Registration by Estimating the Polyphase Decomposition of the Cross-Power Spectrum," *Proceedings Computer Vision and Pattern Recognition 1996*, 532-537.

53. R.C. Hardie, K.J. Barnard, and E.E. Armstrong, "Joint MAP Registration and High-Resolution Image Estimation Using a Sequence of Undersampled Images," *IEEE Transactions on Image Processing*, Vol.6, No. 12, December 1997, 1621-1633.

54. R.J. Althof, M.G.J. Wind, and J.T. Dobbins, "A Rapid and Automatic Image Registration Algorithm with Subpixel Accuracy," *IEEE Transactions on Medical Imaging*, Vol.16, No. 3, June 1997, 308-316.

55. "Special Issue on Image Registration," edited by A. Goshtasby and J. Le Moigne, *Pattern Recognition*, Vol. 32, No.1, January 1999.

56. M. Boddy, J. White, R. Goldman, and N.M. Short, "Planning for Image Processing," in *Proceedings of the Goddard Conference on Space Applications of Artificial Intelligence*, NASA Goddard, Greenbelt, May 10-12, 1994.

57. S. Mallat, and S. Zhong, "Characterization of Signals from Multiscale Edges," *IEEE Transaction on Pattern Analysis and Machine Intelligence*, vol. 4, no.7, pp. 71-732, July 1992.

58. C. Chui, *Introduction To Wavelets*, New York: Academic Press, 1992.

59. I. Daubechies, I., *Ten Lessons on Wavelets*, CMBS-NSF Series Applications in Mathematics, SIAM, 1991.

60. G. Strang, "Wavelets and Dilation Equations: A Brief Introduction," *SIAM Review*, vol. 31, no. 4, pp. 614-627, 1989.

61. S. Mallat, S., "A Theory for Multiresolution Signal Decomposition," *IEEE Pattern Analysis and Machine Intelligence*, vol. PAMI-11, no. 7, 1989.

62. H.S. Stone, J. Le Moigne, and M. McGuire, 1999, "Image Registration Using Wavelet Techniques," *IEEE Transactions on Pattern Analysis and Machine Intelligence*, PAMI, Vol. 21, No.10, October 1999.

63. D. Casasent, D., R. Shenoy, "New Gabor Wavelets with Shift-Invariance for Improved Time-Frequency Analysis and Signal Detection," in *Proceedings 1996 SPIE Wavelet Applications Conference*, Orlando, Florida: p. 244-255, 1996.

64. E.P. Simoncelli, W.T. Freeman, E.H. Adelson, and D.J. Heeger, "Shiftable Multiscale Transforms," *IEEE Transactions on Information Theory*, vol. 38, pp. 587-607, 1992.

65. R.R. Coifman, and D.L. Donoho, "Translation-Invariant De-Noising," *Wavelets and Statistics Lecture Notes*, ed. A. Antoniadis, Springer Verlag, 1995.

66. J. Le Moigne, "Parallel Registration of Multi-Sensor Remotely Sensed Imagery Using Wavelet Coefficients," in *Proceedings 1994 SPIE Wavelet Applications Conf.*, Orlando, pp. 432-443, 1994.

67. J. Le Moigne, J., "Towards a Parallel Registration of Multiple Resolution Remote Sensing Data," in *IGARSS'95, International Geoscience and Remote Sensing Symposium*, Firenze, Italy, July 10-14, 1995.

68. T. El-Ghazawi and J. Le Moigne, "Wavelet Decomposition on High-Performance Computing Systems," in *25-th International Conference on Parallel Processing (ICPP'96)*, Bloomingdale, IL, August 1996.

69. A.K. Chan, C. Chui, J. Le Moigne, H.J. Lee, J.C. Liu, and T.A. El-Ghazawi, "The Performance Impact of Data Placement for Wavelet Decomposition of Two-Dimensional Image Data on SIMD Machines," *Frontiers'95, Fifth Symposium on the Frontiers of Massively Parallel Computation*, McLean, VA, Feb. 6-9, 1995.

70. T. El-Ghazawi, P. Chalermwat, and J. Le Moigne, "Wavelet-Based Image Registration on Parallel Computers," *Supercomputing'97*, San Jose, November 1997.

71. G.W. Rosborough, D.G. Baldwin, W.J. Emery, "Precise AVHRR Image Navigation," *IEEE Transactions on Geoscience and Remote Sensing*, Vol. 32, No. 3, May 1994.

72. D. Baldwin, W. Emery, "Spacecraft Attitude Variations of NOAA-11 Inferred from AVHRR Imagery," *International Journal of Remote Sensing*, Vol. 16, No. 3, 531-548, 1995.

73. J. Le Moigne, W. Xia, J.C. Tilton, T. El-Ghazawi, M. Mareboyana, N. Netanyahu, W.J. Campbell, and R.F. Cromp, 1998, "First Evaluation of Automatic Image Registation Methods," *IGARSS'98, International Geoscience and Remote Sensing Symposium*, July 6-10, 1998.

74. D.M. Mount, N.S. Netanyahu, and J. Le Moigne, 1999, "Efficient Algorithms for Robust Feature Matching," *Special Issue of Pattern Recognition on Image Registration*, Vol. 32, No. 1, pps.17-38, January 1999.

75. N.G. Kinsgbury, "Shift Invariant Properties of the Dual-Tree Complex Wavelet Transforms," *Proceedings of the IEEE International Conference on Acoustics, Speech and Signal Processing (ICASSP)*, Phoenix, March 16-19, 1999.

76. J. Le Moigne, A. Cole-Rhodes, R. Eastman, K. Johnson, J. Morisette, N. Netanyahu, and I. Zavorin, "Multi-Sensor Registration of Earth Remotely Sensed Imagery," *Proceedings of the 8-th SPIE International Symposium on Remote Sensing*, Toulouse, France, September 17-21, 2001.

77. G. Wolberg and S. Zokai, "Robust Image Registration Using Log-Polar Transform," *Proceedings of IEEE International Conference on Image Processing*, Vancouver, Canada, September 2000.

78. H.S. Stone, "Progressive Wavelet Correlation Using Fourier Methods," *IEEE Transactions on Signal Processing*, Vol. 47, No. 1, pp. 97-107, January 1999.

79. J. Le Moigne, and I. Zavorin, "Use of Wavelets for Image Registration," *SPIE Aerosense 2000, "Wavelet Applications VII"*, Orlando, FL, April 24-28, 2000.

Rows   *Columns*

F   represents the convolution of the input image by the filter F
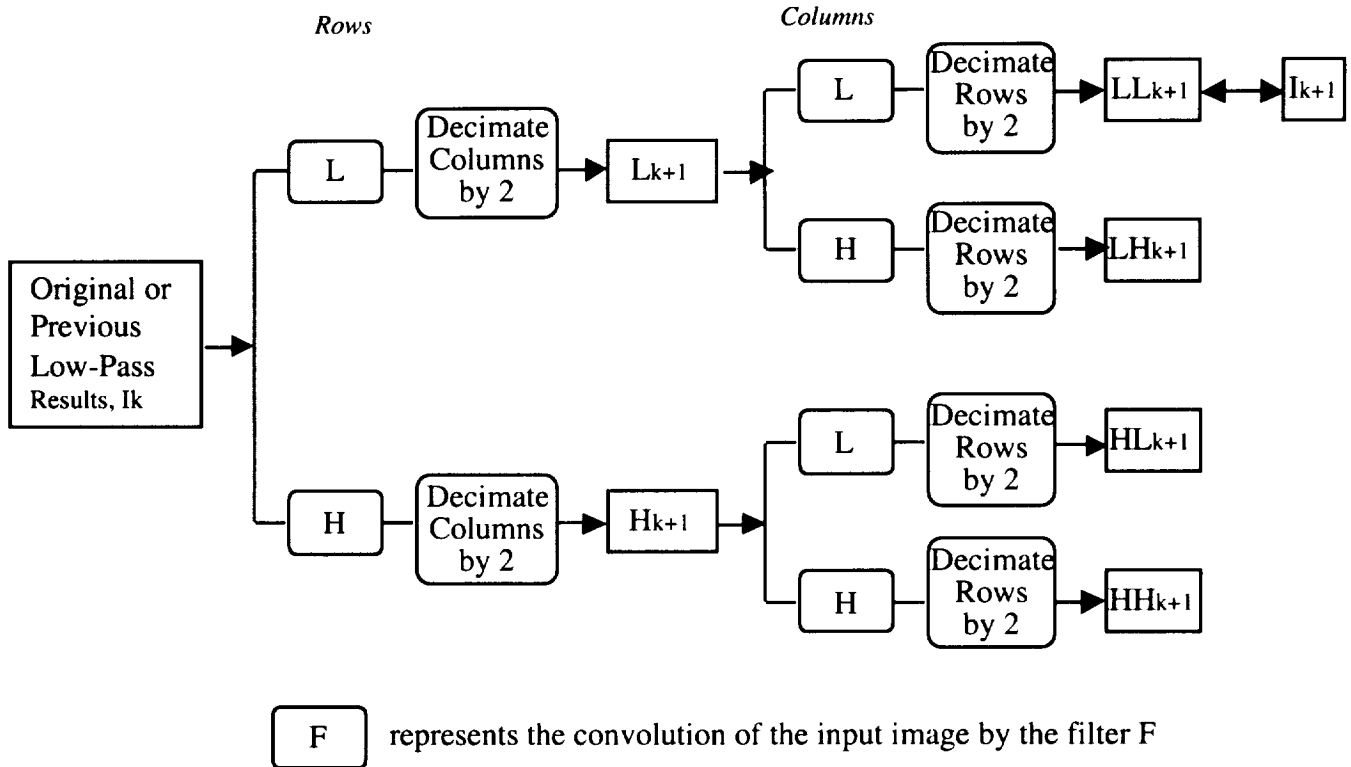
Figure 1
Decomposition by an Orthonormal Basis of Wavelets

Decomp. Level	Search Interval	Accuracy	Result Rotation
n	$[0 ; \Pi/2]$	$2^{n-1}\delta$	R_n
n-1	$[R_n - 2^{n-1}\delta ; R_n + 2^{n-1}\delta]$	$2^{n-2}\delta$	R_{n-1}
n-2	$[R_{n-1} - 2^{n-2}\delta ; R_{n-1} + 2^{n-2}\delta]$	$2^{n-3}\delta$	R_{n-2}
...	...	...	...
2	$[R_3 - 2^2\delta ; R_3 + 2^2\delta]$	2δ	R_2
1	$[R_2 - 2\delta ; R_2 + 2\delta]$	δ	R_1

Table 1
Iterative Rotation Registration Using n Wavelet Decomposition Levels

Wavelet Level	Reference Wavelet Coefficients	Rotations of Reference Wavelet Coefficients	Input Wavelet Coefficients	Result: Rotation with Best Correlation
4	32 X 32 LH4r and HL4r Wavelet Images (Level 4)	Rotate both LH4 r and HL4r by all rotations in [0,90°] at a step of 10°.	Correlate Input Wavelet Images LH4i (resp. HL4i) with all rotated LH4r (resp. HL4r).	R_4
3	64 x 64 LH3r and HL3r Wavelet Images (Level 3)	Rotate both LH3 r and HL3r by all rotations in [R_4-10°,R_4+10°] at a step of 5°.	Correlate Input Wavelet Images LH3i (resp. HL3i) with all rotated LH3r (resp. HL3r).	R_3
2	128 X 128 LH2r and HL2r Wavelet Images (Level 2)	Rotate both LH2 r and HL2r by all rotations in [R_3-5°,R_3+5°] at a step of 2°.	Correlate Input Wavelet Images LH2i (resp. HL2i) with all rotated LH2r (resp. HL2r).	R_2
1	256 X 256 LH1r and HL1r Wavelet Images (Level 1)	Rotate both LH1 r and HL1r by all rotations in [R_3-2°,R_3+2°] at a step of 1°.	Correlate Input Wavelet Images LH1i (resp. HL1i) with all rotated LH1r (resp. HL1r).	R_1

Table 2
Registration Algorithm - Search for Rotations,
for a 512x512 image, 4 levels of decomposition, accuracy=1 degree

Level	Image Size	Feature Space	Search Space Rotation	Search Space Translation	Result	card(search sp) (if $\delta T = \delta\Theta = 1$)
4	32 X 32	LH and HL Wave Coeff. (Level 4)	[0,10] (degrees) with accuracy of 4 degrees	[0,16] X [0,16] with accuracy of 4 pixels	$(Tx4, Ty4, \Theta_4)$	3*5*5=75
3	64 x 64	LH and HL Wave Coeff. (Level 3)	{$\Theta4$}	[2*Tx4-10,2*Tx4+10] X [2*Ty4-10,2*Ty4+10] with accuracy of δT *4	$(Tx3, Ty3, \Theta_4)$	6*6=36
			[$\Theta4$ – 10, $\Theta4$ + 10] with accuracy of $\delta\Theta$* 4	{Tx3} X {Ty3}	$(Tx3, Ty3, \Theta_3)$	6 (would be 6*6*6= 216 if direct search)
2	128 X 128	LH and HL Wave Coeff. (Level 2)	{$\Theta3$}	[2*Tx3-5,2*Tx3+5] X [2*Ty3-5,2*Ty3+5] with accuracy of δT *2	$(Tx2, Ty2, \Theta_3)$	6*6=36
			[$\Theta3$ – 5, $\Theta3$ + 5] with accuracy of $\delta\Theta$ * 2	{Tx2} X {Ty2}	$(Tx2, Ty2, \Theta_2)$	6 (would be 6*6*6= 216 if direct search)
1	256 X 256	LH and HL Wave Coeff. (Level 1)	[$\Theta2$ – 2, $\Theta2$ + 2] with accuracy of $\delta\Theta$	[2*Tx2-2,2*Tx2+2] X [2*Ty2-2,2*Ty2+2] with accuracy of δT	$(Tx1, Ty1, \Theta_1)$	5*5*5=125 Total = 284 (instead of 632)

Table 3
Registration Algorithm - Search for Composition of Translations and Rotations,
for a 512x512 image, 4 levels of decomposition, accuracies = $\delta\Theta$ degrees and δT pixels.

Filter Size	Levels of Decomposition	Sequential Timing (sec.)	Parallel Timing (sec.)
2	1	3.13	0.0109
	2	3.61	0.0114
	3	3.91	0.1190
	4	4.41	0.0123
4	1	3.99	0.0120
	2	4.54	0.0138
	3	4.88	0.0146
	4	4.87	0.0154
6	1	4.50	0.0148
	2	5.91	0.0163
	3	6.07	0.0174
	4	5.98	0.0186
8	1	5.47	-
	2	7.12	0.0188
	3	7.55	0.0203
	4	7.55	0.0218
10	1	6.57	0.0188
	2	7.90	0.0212
	3	8.86	0.0231
	4	8.92	0.0250
12	1	17.43	0.0286
	2	21.21	0.0333
	3	21.99	0.0369
	4	23.31	0.0407

Table 4

Timings for the Wavelet Decomposition of a 512x512 Image;
Parallel Implementation on the MasPar MP-2

PE #	Cray T3E	Cray T3D	Beowulf
1	2.382	6.709	4.664
2	1.303	4.284	2.390
4	0.604	2.022	1.279
8	0.330	0.896	0.739
16	0.196	0.520	0.545

Table 5

Timings for the Wavelet Registration of a 512x512 Image;
Parallel Implementations on Cray T3D, Cray T3E and Beowulf high-performance architectures
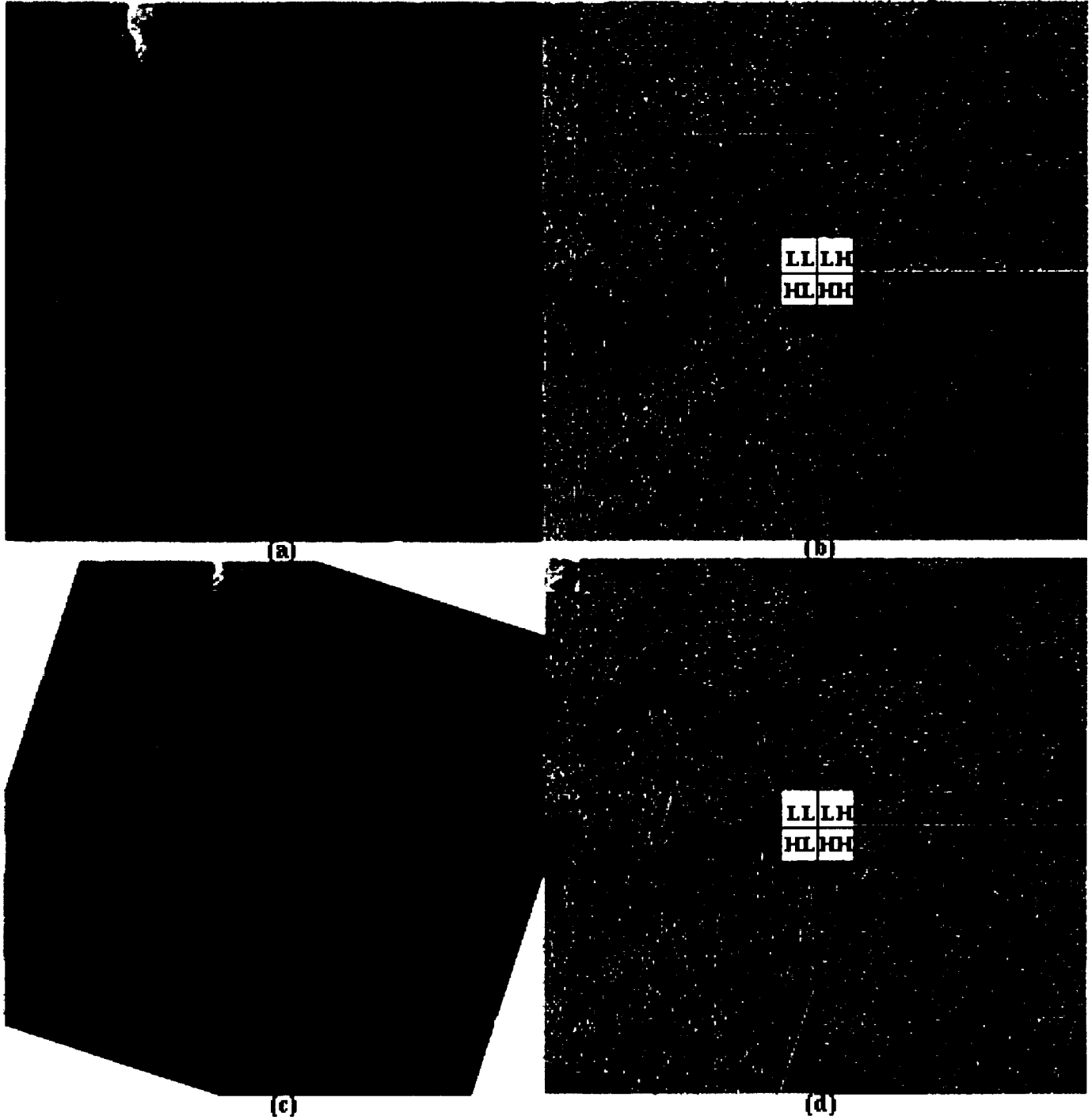
Figure 2
(a) *Original Landsat-Thematic Mapper Image*
   (Pacific Northwest)
(b) *Wavelet Coefficients Corresponding to Figure 1a*
(c) *Figure 1a Rotated by 18 Degrees*
(d) *Wavelet Coefficients Corresponding to Figure 1c*

LEVEL 4 - Search for Rotations in [0,88 degrees]

Rotations of Reference LH's

Input LH

Rotations of Reference HL's

Input HL

---> Best Rotation at Level 4 : 16 degrees

LEVEL 3 - Search for Rotations in [6,26 degrees]

Rotations of Reference LH's

Input LH

Rotations of Reference HL's

Input HL

---> Best Rotation at Level 3 : 18 degrees
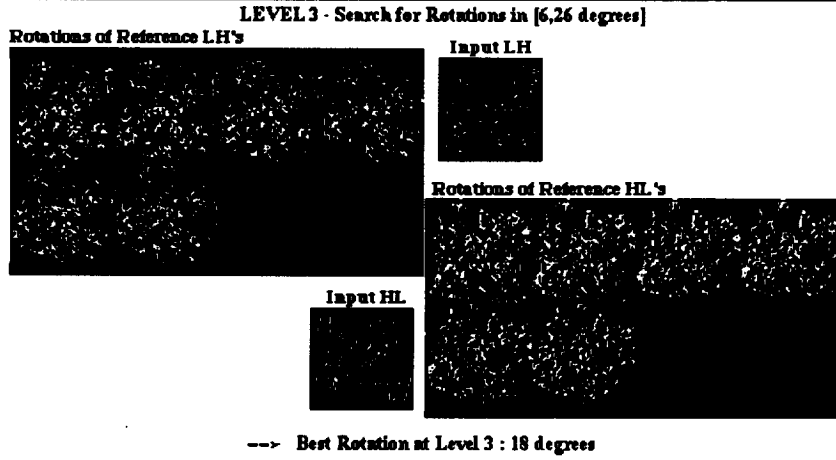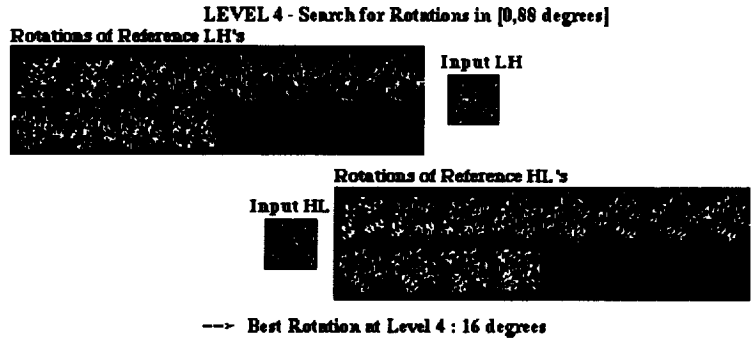
Figure 3a
Maxima of Wavelet coefficients for Level 4 (32x32) and Level 3 (size 64x64)

Rotations of Reference LH's : Level 2

Input LH : Level 2

---> Best Rotation at
Level 2 : 19 degrees
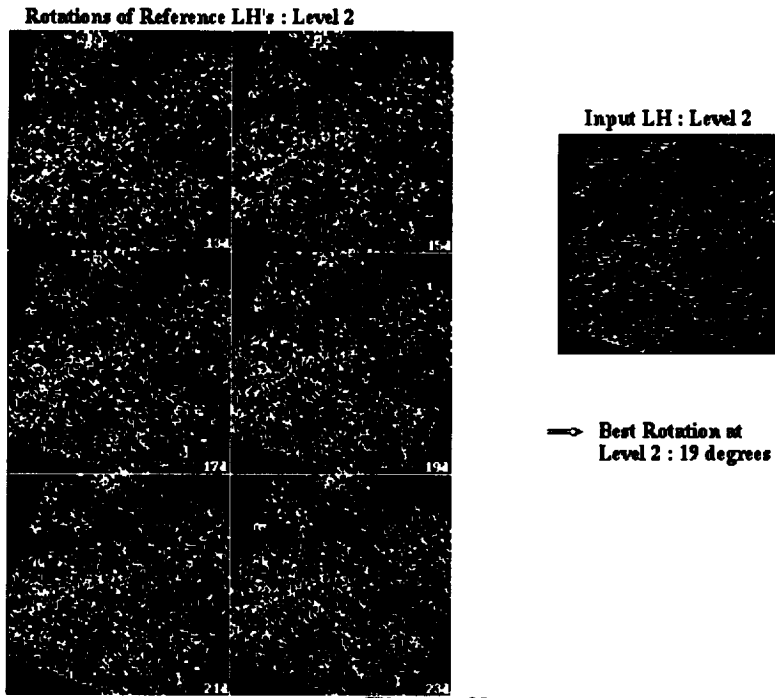
Figure 3b
Maxima of Wavelet coefficients - Level 2 (size 128x128)
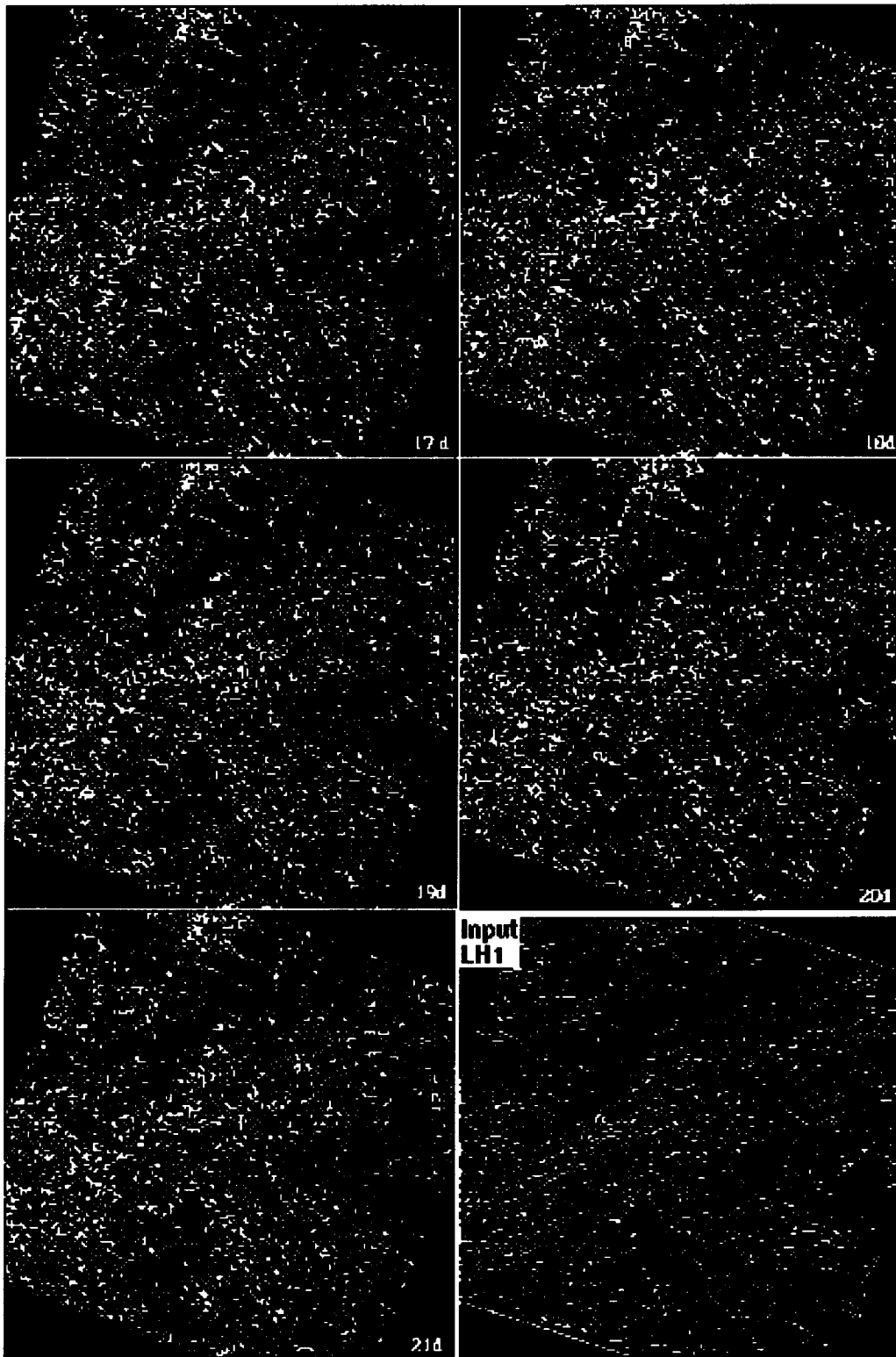
Best Rotation at Level 1 : 18 Degrees

Figure 3c - *Maxima of Wavelet coefficients for Level 1 (size 256x256) for Reference Images Rotated 17,18,19,20, and 21 degrees and Compared t o the Input Image*
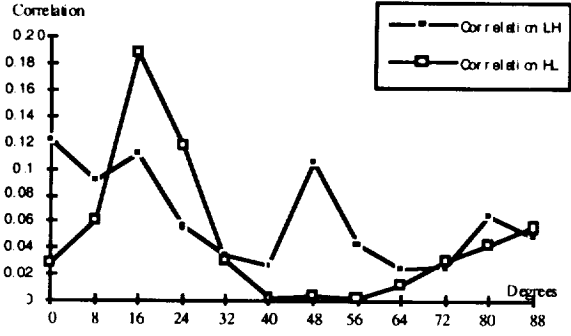
Figure 4a
Correlation Functions - Level 4
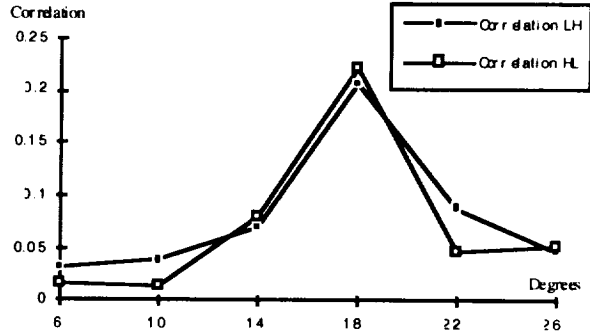

Figure 4b
Correlation Functions - Level 3
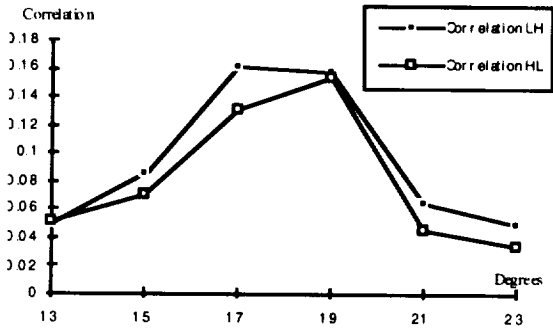

Figure 4c
Correlation Functions - Level 2
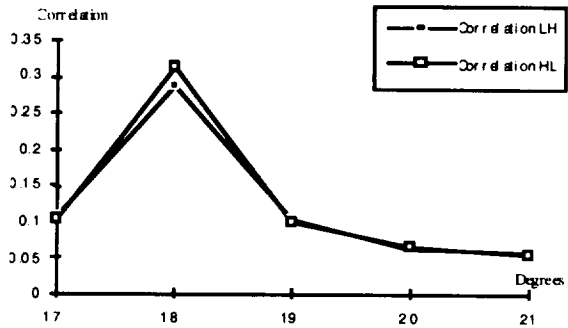
Figure 4d
Correlation Functions - Level 1

Rotation (degrees)	Translation (TX,TY)	"x" Values	Correlation	Computed "x"
0	(100,0)	5%	0.18	
		10%	0.19	
		15%	0.32	
		20%	0.22	0.13
0	(0,50)	5%	0.36	
		10%	0.52	
		15%	0.59	
		20%	0.53	0.13
0	(20,60)	5%	0.13	
		10%	0.29	
		15%	0.39	
		20%	0.34	0.14
5	(100,0)	5%	0.19	
		10%	0.21	
		15%	0.27	
		20%	0.29	0.13
5	(0,50)	5%	0.37	
		10%	0.48	
		15%	0.51	
		20%	0.38	0.13
5	(20,60)	5%	0.07	
		10%	0.19	
		15%	0.3	
		20%	0.35	0.15

Table 6
Adaptive Choice of Wavelet Histogram Threshold

DATA	GIRL					TM						
True Rotation	5	55	5	5	0	18	18	4	4	4	0	0
True Translation	(0,0)	(0,0)	(20,60)	(6,4)	(20,60)	(0,0)	(0,50)	(0,0)	(50,0)	(5,2)	(50,0)	(5,2)
SPATIAL CORRELATION (Only) Translation (pixels)	-	-	-	-	(20,61)	-	-	-	-	-	(50,0)	(5,2)
PHASE CORRELATION (Only) Translation (pixels)	-	-	-	-	(20,60)	-	-	-	-	-	(50,0)	(5,2)
ITER EDGE MATCHING Rotation (degrees)	5	55	5	5	3	18	18	4	4	4	-1	0
Translation (pixels)	(0,0)	(0,0)	(20,60)	(6,4)	(19,61)	(0,1)	(0,51)	(0,0)	(50,0)	(5,2)	(49,0)	(5,2)
WAVELET REGISTRATION Rotation (degrees)	5	55	5	5	0	18	23	4	4	4	0	0
Translation (pixels)	(0,0)	(0,0)	(20,60)	(6,4)	(20,60)	(0,0)	(0,50)	(0,0)	(50,0)	(4,2)	(50,0)	(6,2)
WAVE-REG: Error Rotation	0	0	0	0	0	0	5	0	0	0	0	0
Error-Translation	0	0	0	0	0	0	0	0	0	1	0	1

Table 7

*Results of our Wavelet-Based Registration Compared to Other Methods and Applied to Two
Test Images (a Portrait, GIRL, see ref [66] and Figure 2a)
for Multiple Rotations and Translations*
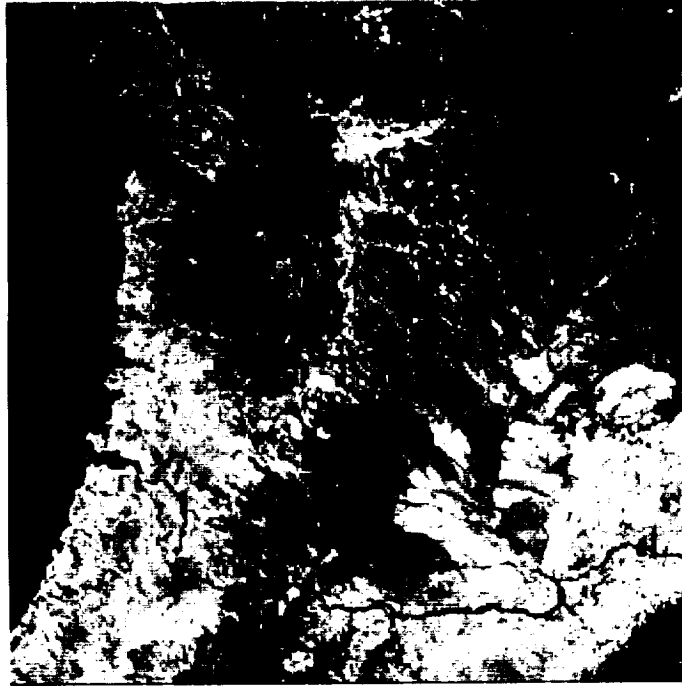
Figure 5
Original AVHRR Image (Pacific Northwest)

```
FIND BEST TRANSFORMATION AT LEVEL 4.
            search theta in [ 0.00,10.00] and (TX,TY) in [ 0.00,16.00]X[ 0.00,16.00],
            with the increment: 4.00

            for the threshold =  0.05 and the rotation =  0.00 Translation_optimal = ( 1.12 ,  0.56)
            for the threshold =  0.10 and the rotation =  0.00 Translation_optimal = ( 1.12 ,  0.56)
            for the threshold =  0.15 and the rotation =  0.00 Translation_optimal = ( 1.12 ,  0.56)
            for the threshold =  0.20 and the rotation =  0.00 Translation_optimal = ( 1.12 ,  0.56)

            for the threshold =  0.05 and the rotation =  4.00 Translation_optimal = ( 0.67 ,  0.00)
            for the threshold =  0.10 and the rotation =  4.00 Translation_optimal = ( 1.33 ,  0.00)
            for the threshold =  0.15 and the rotation =  4.00 Translation_optimal = ( 1.75 ,  0.00)
            for the threshold =  0.20 and the rotation =  4.00 Translation_optimal = ( 1.75 ,  0.59)

            for the threshold =  0.05 and the rotation =  8.00 Translation_optimal = ( 0.40 ,  0.00)
            for the threshold =  0.10 and the rotation =  8.00 Translation_optimal = ( 0.40 ,  0.00)
            for the threshold =  0.15 and the rotation =  8.00 Translation_optimal = ( 1.07 ,  0.00)
            for the threshold =  0.20 and the rotation =  8.00 Translation_optimal = ( 2.13 ,  0.00)

            At level 4,    Rotation_optimal =  0.00 and Translation_optimal = ( 1.00 ,  0.00)
                                 and the Correlation is : 0.312404


FIND BEST TRANSFORMATION AT LEVEL 3
            search theta in [-8.00, 8.00], (TX,TY) in [-6.00,10.00]X[-8.00, 8.00]
            with the increment: 4.00 and the threshold: 0.11

            At level 3,    Rotation_optimal =  8.00 and Translation_optimal = ( 2.00 ,  0.00)
                                 and the Correlation is : 0.202801


FIND BEST TRANSFORMATION AT LEVEL 2
            search theta in [ 4.00,12.00], (TX,TY) in [ 0.00, 8.00]X[-4.00, 4.00]
            with the increment: 2.00 and the threshold: 0.09

            At level 2,    Rotation_optimal =  6.00 and Translation_optimal = ( 2.00 ,  2.00)
                                 and the Correlation is : 0.238743


FIND BEST TRANSFORMATION AT LEVEL 1
            search theta in [ 4.00, 8.00], (TX,TY) in [ 2.00, 6.00]X[ 2.00, 6.00]
            with the increment: 1.00 and the threshold: 0.07

            At level 1,    Rotation_optimal =  5.00 and Translation_optimal = ( 5.00 ,  3.00)
                                 and the Correlation is : 0.648763


INTERPOLATION TO FULL IMAGE: Rotation =  5.00 and (TX,TY) = (10.00, 6.00)
```

Table 8
Results of our Automatic Wavelet-Based Registration Applied to Figure 3
*Search for Compositions of Rotations and Translations*
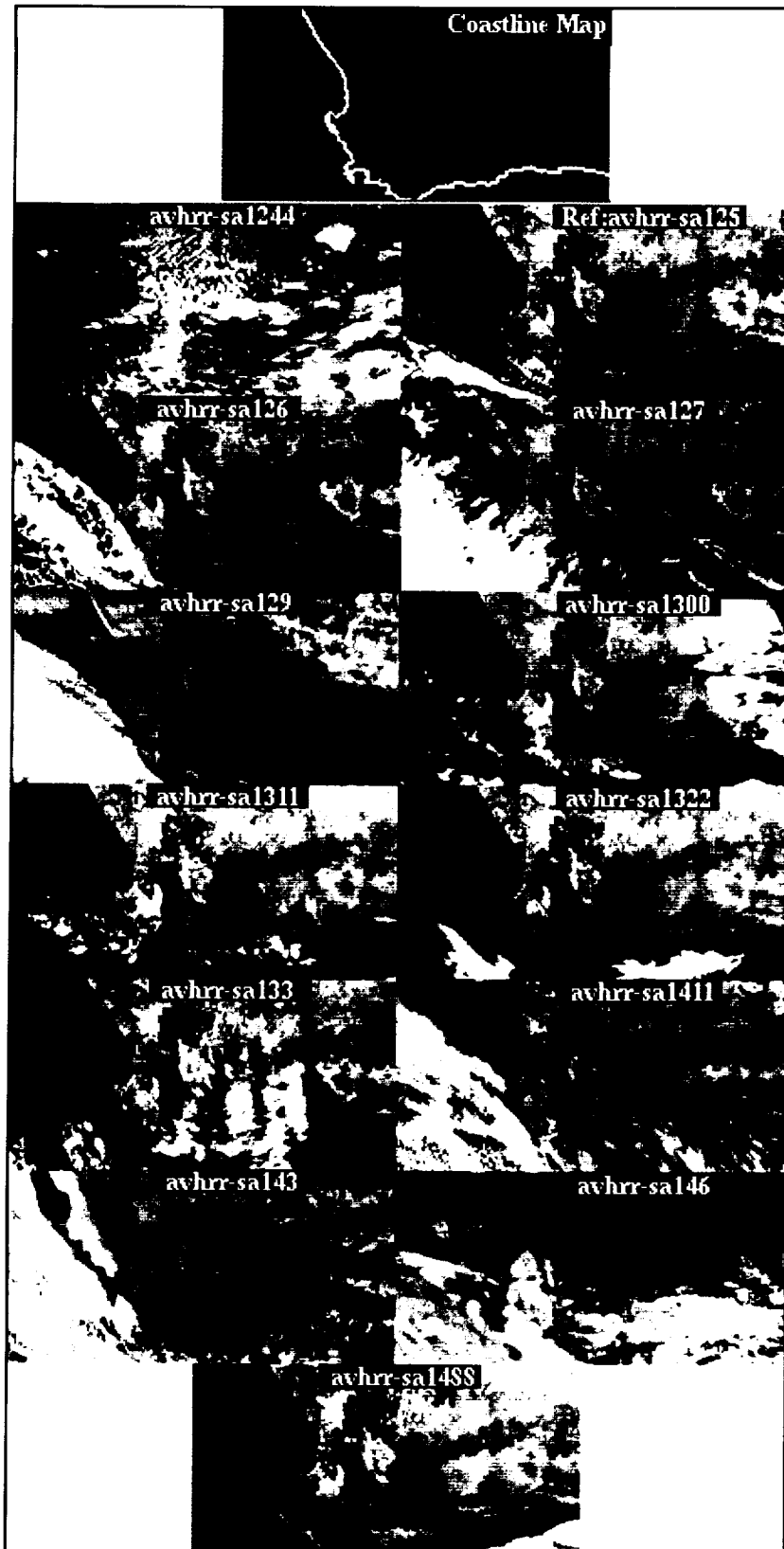
**Figure 6 - *Third Dataset - Coastline Map and Thirteen Images
of a Multi-Temporal Series of AVHRR-LAC Band 2 Images over South Africa***

Manual

Wavelet

Extracted from avhrr sa126   Extracted from avhrr sa1488
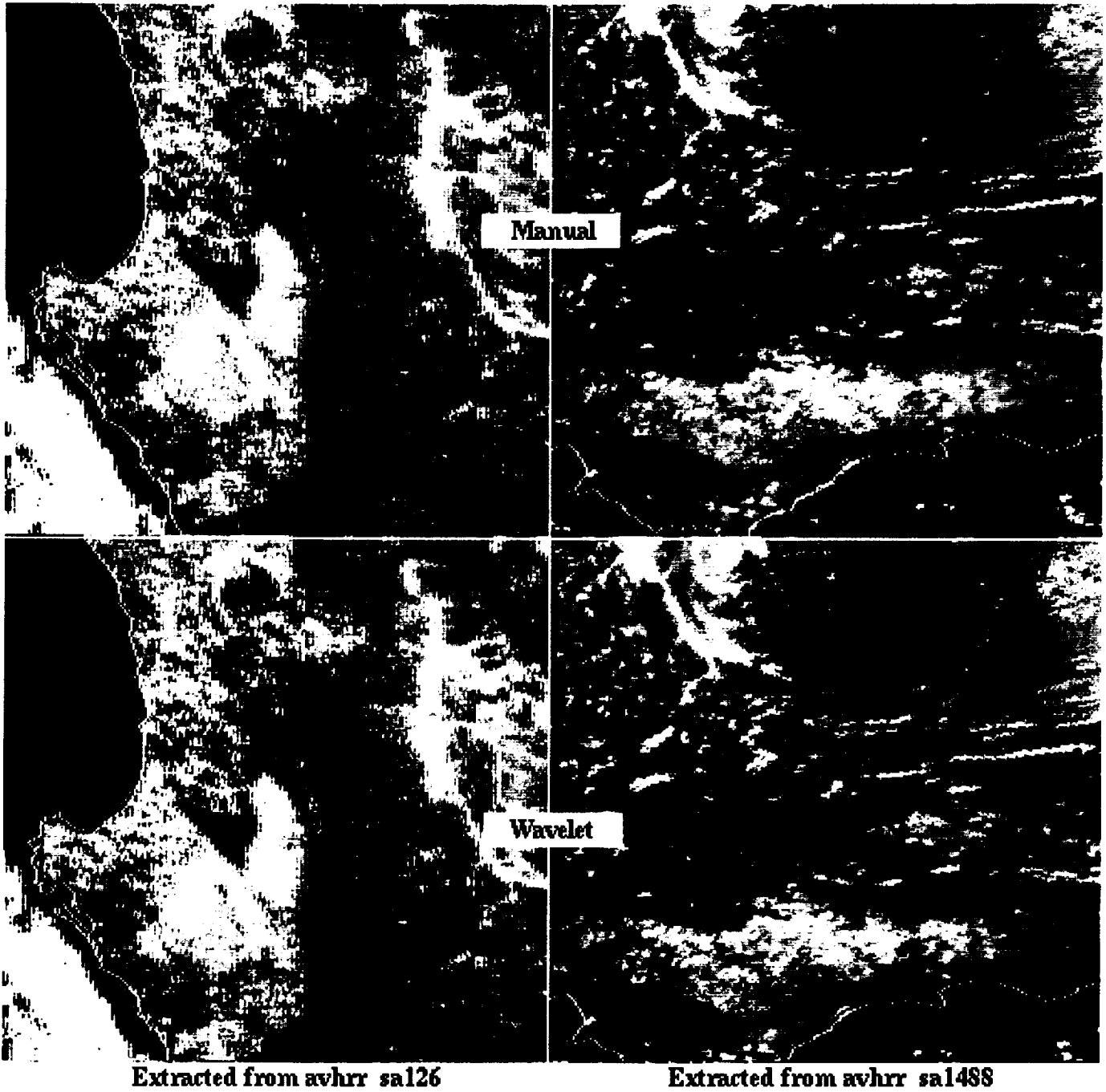
Figure 7
Zoom on Coastlines Transformed by Wavelet-Registration ,
Superimposed for Two of the AVHRR Images, "avhrr_sa126, avhrr_sa1488"
and Compared to the Manual Registration Results

AVHRR DATA	sa1244	sa126	sa127	sa129	sa1300	sa1311	sa1322	sa133	sa1411	sa143	sa146	sa1488
MANUAL REGISTRATION												
Rotation	0	0	0	0	0	0	0	0	0	0	0	0
Translation	(1,0)	(0,0)	(-1,-1)	(-3,-1)	(2,0)	(1,0)	(0,-1)	(0,-1)	(0,-1)	(-1,-3)	(-3,-5)	(2,3)
WAVELET REGISTRATION												
Rotation	0	0	0	-1	0	0	0	0	0	0	-2	0
Translation	(0,0)	(0,0)	(0,-2)	(-6,-2)	(4,0)	(2,0)	(0,-2)	(0,-2)	(0,-2)	(0,-4)	(-6,-6)	(2,4)

Table 9
Results of the Wavelet-Based Registration on the AVHRR Dataset Over South Africa

NASA Scientific and Technical Document Availability Authorization (DAA)

National Aeronautics and Space Administration

☐ Original
☐ Modified

I. DOCUMENT/PROJECT IDENTIFICATION

TITLE

An Automated Parallel Image Registration Technique Based on The Correlation of Wavelet Features

AUTHOR(S)

Jacqueline Le Moigne
William J. Campbell
Robert F. Cromp

ORIGINATING NASA ORGANIZATION

NASA/Goddard Space Flight Center

PERFORMING ORGANIZATION *(If different)*

Code 935

CONTRACT/GRANT/INTERAGENCY/PROJECT NUMBER(S)	DOCUMENT NUMBER(S)	DOCUMENT DATE

For presentations, documents, or other STI to be externally published (including through electronic media), enter appropriate information on the intended publication such as name, place, and date of conference, periodical, or journal name, or book title and publisher in the next box. These documents must be routed to the NASA Headquarters or Center Export Control Administrator for approval (see Sections III and VIII).

II. SECURITY CLASSIFICATION

CHECK ONE *(One of the five boxes denoting Security Classification must be checked.)*

☐ SECRET   ☐ SECRET RD   ☐ CONFIDENTIAL   ☐ CONFIDENTIAL RD   ☒ UNCLASSIFIED

III. AVAILABILITY CATEGORY

☐ ITAR   ☐ EAR

Export Controlled Document - USML Category Classification Number (ECCN) /CCL Export Control *(Documents marked in this block must have the concurrence/approval of the NASA Headquarters or Center Export Control Administrator (see Section VIII).)*

Confidential Commercial Document *(check appropriate box at left and indicate below the appropriate limitation and expiration):*

☐ TRADE SECRET
☐ SBIR
☐ COPYRIGHTED

☐ U.S. Government agencies and U.S. Government agency contractors only
☐ NASA contractors and U.S. Government only
☐ U.S. Government agencies only
☐ NASA personnel and NASA contractors only
☐ NASA personnel only
☐ Available only with the approval of issuing office:
☐ Limited until *(date)*

☒ PUBLICLY AVAILABLE

Publicly available documents must be unclassified, may not be export controlled, may not contain trade secret or confidential commercial data, and should have cleared any applicable patents application process.

IV. DOCUMENT DISCLOSING AN INVENTION

THIS DOCUMENT MAY BE RELEASED ON *(date)*	NASA HQ OR CENTER PATENT OR INTELLECTUAL PROPERTY COUNSEL SIGNATURE	DATE

V. BLANKET RELEASE (OPTIONAL)

☐ All documents issued under the following contract/grant/project number may be processed as checked in Sections II and III.

☐ The blanket release authorization granted on *(date)*

☐ is RESCINDED - Future documents must have individual availability authorizations.

☐ is MODIFIED - Limitations for all documents processed in the STI system under the blanket release should be changed to conform to blocks as checked in Sections II and III.

NASA FORM 1676 AUG 97

PLEASE CONTINUE ON REVERSE SIDE.

ABSTRACT

With the increasing importance of multiple platform/multiple remote sensing missions, fast and automatic integration of digital data from disparate sources has become critical to the success of these endeavors. Our work utilizes maxima of wavelet coefficients to form the basic features of a correlation-based automatic registration algorithm. Our wavelet-based registration algorithm is tested successfully with data from the NOAA Advanced Very High Resolution Radiometer (AVHRR) and the Landsat/Thematic Mapper (TM), which differ by translation and/or rotation. By the choice of high-frequency wavelet features, this method is similar to an edge-based correlation method, but by exploiting the multi-resolution nature of a wavelet decomposition, our method achieves higher computational speeds for comparable accuracies. This algorithm has been implemented on a Single Instruction Multiple Data (SIMD) massively parallel computer, the MasPar MP-2, as well as on the CrayT3D, the Cray T3E and a Beowulf cluster of Pentium workstations.